Broken Cloud Field Longwave Scattering Effects

E. E. Takara and R. G. Ellingson
University of Maryland
College Park, Maryland

Introduction

Many general circulation models simplify longwave radiative transfer calculations by neglecting the geometry of broken cloud fields. Quantities are computed by weighting the clear sky and completely overcast results by the fractional cloud cover. This treats broken cloud fields as sets of flat plates. Ice clouds are assigned a reflectivity and emissivity. Water clouds are assumed to be black.

It has been shown (Ellingson 1982; Harshvardhan and Weinman 1982; Killen and Ellingson 1994) that the flatness assumption fails for water clouds. Longwave scattering by the water clouds was neglected since it was assumed that the clouds were effectively black. In Takara and Ellingson (1996), longwave scattering effects were of the same magnitude as geometric effects when gaseous absorption was neglected. This is an extension of that work, modeling the longwave scattering effects of single broken cloud layers in typical atmospheres.

Computation

Gaseous absorption was neglected in Takara and Ellingson because absorption in the 8 to 12-μm window is small compared with the rest of the longwave range. Though the window is relatively clear, water vapor absorption can be significant in some cases. With that in mind, the window was divided into six intervals. The upward and downward radiances were computed by summing over the intervals.

$$I^{\uparrow\downarrow} = \int_{8\ \mu m}^{12\ \mu m} I_\lambda^{\uparrow\downarrow}\, d\lambda = \sum_{i=1}^{6} I_i^{\uparrow\downarrow}\, \Delta\lambda \qquad (1)$$

The intervals are

$$8\ \mu m < \lambda_1 < 8.25\ \mu m < \lambda_2 < 8.75\ \mu m < \lambda_3 < 9.25\ \mu m$$
$$9.25\ \mu m < \lambda_4 < 10 \mu m < \lambda_5 < 11\ \mu m < \lambda_6 < 12\ \mu m$$

The upward and downward fluxes are found by Gaussian quadrature of the radiances. Heating rates are computed from the fluxes.

Upward and downward radiances above and below the cloud layer are functions of gaseous transmission and emission. The upward and downward radiances at zenith angle θ and altitudes $Z_i > Z_j$ are

$$I^{\uparrow}(Z_i, \theta) = T(Z_i, Z_j, \theta)\, I^{\uparrow}(Z_j) + E(Z_j, Z_i, \theta) \qquad (2a)$$

$$I^{\downarrow}(Z_j, \theta) = T(Z_i, Z_j, \theta)\, I^{\downarrow}(Z_i) + E(Z_i, Z_j, \theta) \qquad (2b)$$

The transmissivities, $T(Z_i, Z_j, \theta)$, and the emissions $E(Z_i, Z_j, \theta)$, $E(Z_j, Z_i, \theta)$ were calculated using the Line-by-Line Radiative Transfer Model (LBLRTM).

The downward radiances below the cloud layer and the upward radiances above the cloud layer are dependent on the radiances exiting the layer. They are a function of the radiative transfer within the cloud layer. Once the cloud layer's outward radiances are known, the dependent radiances are found using (2a,b). The upward radiances below the clouds and the downward radiances above the clouds are independent of the cloud layer. They were pre-computed by LBLRTM and tabulated.

The cloud layer outward radiances are a function of the radiances entering the layer and the layer's physical properties. The Monte Carlo method was used to model the radiative transfer. Photon bundles were emitted at Gaussian angles at the bottom and top of the cloud layer and tracked until absorption or escape.

Assumptions and Parameters

Four assumptions were made in the computations. First, the cloud field was a single layer of identical randomly overlapping cylinders with a constant cloud base altitude. Second, the

clouds were homogenous. Third, the clouds had the same temperature profile as the surrounding air. Last, the temperature variation between levels was assumed to be linear. The McClatchey soundings were used for temperature and species profiles. Results for the tropical (TRP) and sub-arctic winter (SAW) soundings, representing highs and lows of temperature and water vapor concentration, are presented here.

The fluxes were computed for various pairs of cloud aspect ratio (α) and cloud diameter (D), with base cloud fraction (N) and cloud base altitude (Z_b). To model small flat clouds, α was 0.5 with a diameter of 0.25 km. For large tall clouds, α = 1 and D = 1 km. The values of N were 0.1, 0.3, 0.5, 0.7, 0.9, and 1. Values of Z_b were 0.5, 2, and 4 km for water clouds, 8, 10, and 12 km for ice clouds.

The cloud extinction coefficient (K_t), single scattering albedo (ω_0), and asymmetry factor (g) within each wavelength interval, were calculated from parameterizations. Hu and Stamnes (1993) was used for water clouds, Fu and Liou (1993) for ice clouds.

The water cloud equivalent radius (R_{eq}) was set at 3, 5, and 10 µm , the liquid water content (LWC) at 0.1 and 1 $g*m^{-3}$ for SAW and TRP. For ice clouds, the equivalent diameters (D_{eq}) ice water content (IWC) pairs were 75 µm, 0.005 $g*m^{-3}$, 93 µm, 0.014 $g*m^{-3}$, and 110 µm, 0.029 $g*m^{-3}$.

The values of K_t, ω_0, and g in the six spectral intervals were fixed at their average value. The water cloud values are shown in Figures 1a and b. As R_{eq} increases, g increases. This increases the forward scattering and makes the water cloud behave more like a blackbody. The ice cloud values are shown in Figures 2a and b. Note that the water clouds are considerably more opaque than the ice clouds.

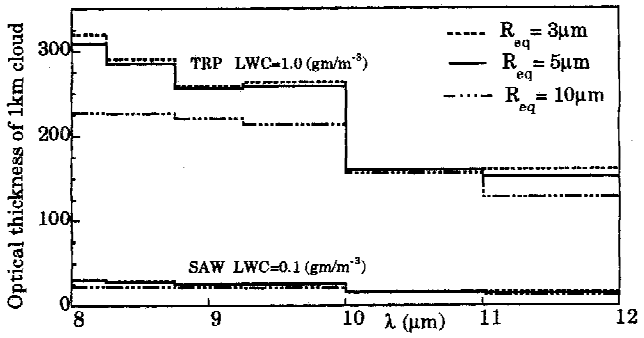

Figure 1a. Optical thicknesses of 1-km thick water clouds, for TRP and SAW.

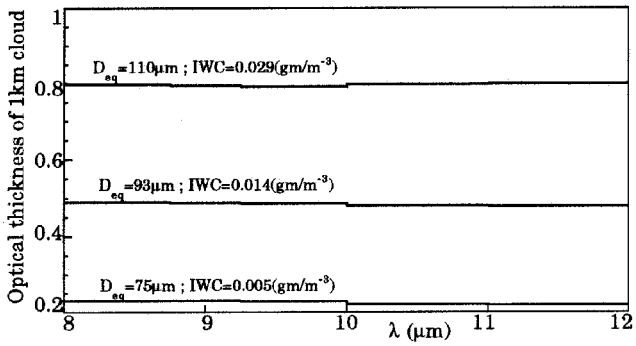

Figure 1b. ω_0 and g for water clouds, various R_{eq}.

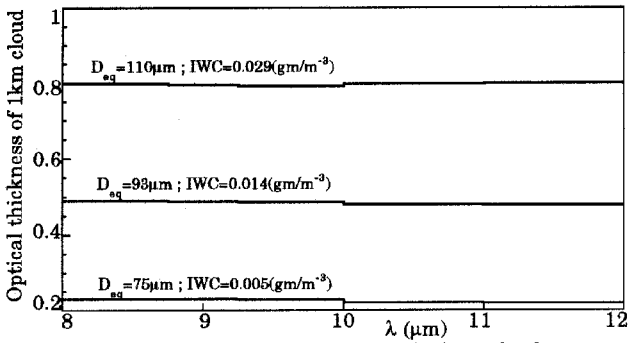

Figure 2a. Optical thickness of 1-km thick ice clouds, for D_{eq} and IWC pairs.

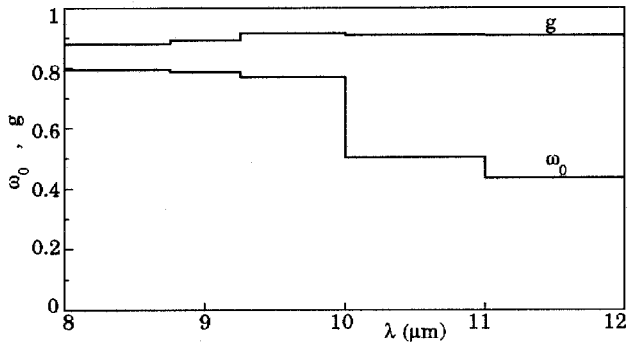

Figure 2b. ω_0 and g for ice clouds.

Results

The downward flux at the surface as a function of base cloud fraction (N) for the TRP and SAW atmospheres is shown in Figures 3a and b. Solid lines were used for the large clouds (α = 1 D = 1 km), dashed lines for the small

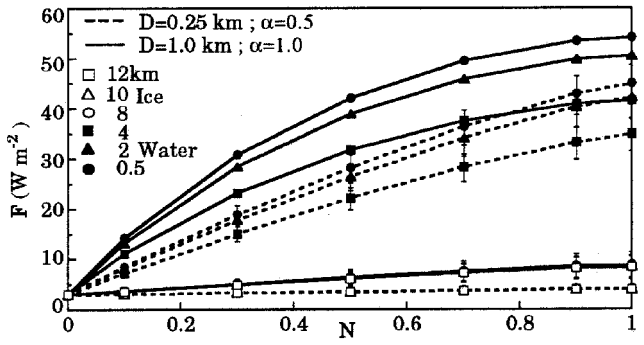

Figure 3a. Tropical downward flux at surface for various cloud geometries and altitudes.

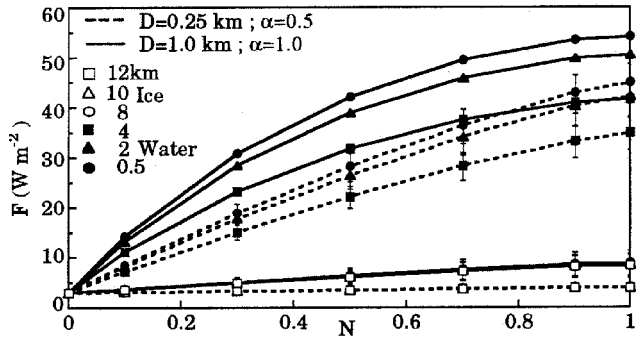

Figure 3b. Sub-arctic winter downward flux at surface for various cloud geometries and altitudes.

clouds (α = 0.5 D = 0.25 km). The solid symbols are for the water clouds with base altitudes of 0.5, 2, and 4 km; the open symbols are for ice clouds with base altitudes of 8, 10, and 12 km. The symbols are centered on the fluxes for R_{eq} = 5 µm ; and D_{eq} = 93 µm IWC = 0.014 $g*m^{-3}$. Limit bars show results for the other R_{eq} and D_{eq}-IWC pairs. These limit bars are quite small in Figure 3a, but more apparent in Figure 3b.

In Figure 3a (TRP), the water cloud fluxes decrease as cloud altitude increases. At smaller values of N, they also decrease with cloud size. In the completely overcast case (N = 1), cloud size has no effect because both the small and large clouds are opaque. Due to the high LWC, changing the microphysical properties has little effect. The variation in flux with R_{eq} is less than $1 W*m^{-2}$. There is little change in the ice cloud fluxes from the clear sky result (N = 0), regardless of cloud altitude, geometry, or microphysical properties. This is the result of the high temperature and water vapor concentration in the lower kilometers; the surface flux is dominated by the lower atmosphere.

In Figure 3b (SAW), the atmosphere is considerably drier and colder, resulting in much lower fluxes. The water clouds behave as in Figure 3a; surface flux decreases with cloud altitude and cloud size. The fluxes no longer match at N = 1 because the small clouds are not opaque. The large water cloud fluxes do not vary with R_{eq}—they are opaque. The small water cloud flux varies with R_{eq}, decreasing as R_{eq} increases. For a completely overcast sky (N = 1), cloud base at 0.5 km (solid circle dashed line R_{eq} = 5 µm), the flux is 45 $W*m^{-2}$ with an upper limit of 49 $W*m^{-2}$ (R_{eq} = 3 µm) and a lower limit of 41 $W*m^{-2}$ (R_{eq} = 10 µm). The ice cloud fluxes vary slightly from the clear sky flux. There is a small increase in flux as the clouds get bigger. Flux variations with D_{eq} and IWC are less than 2 $W*m^{-2}$.

The upward flux at 15 km for TRP and SAW is shown in Figures 4a and b. In Figure 4a, the water cloud fluxes decrease as cloud height increases. The smaller clouds have higher fluxes because their cloud top temperatures are higher. As in Figure 3a, the variation with R_{eq} is less than 1 $W*m^{-2}$. The ice cloud fluxes group together according to cloud size. The small cloud fluxes are closely bunched,

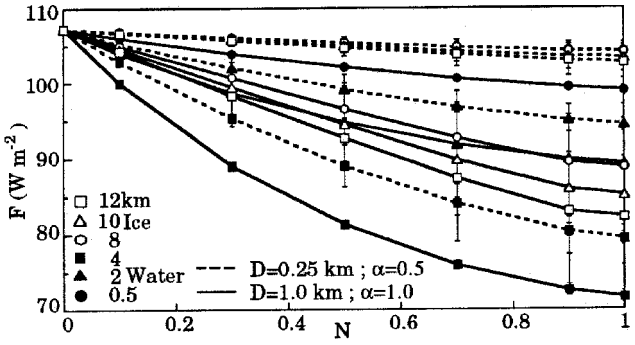

Figure 4a. Tropical upward flux at 15 km for various cloud geometries and altitudes.

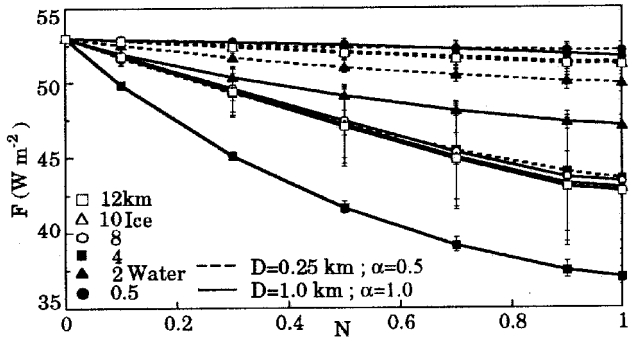

Figure 4b. Sub-arctic winter upward flux at 15 km for various cloud geometries and altitudes.

close to the clear sky flux, decreasing as cloud altitude and N increase. They do not show much dependence on D_{eq} and

IWC because their optical thickness is quite small (< 0.1) for the small clouds. The large ice cloud fluxes are also bunched, decreasing as cloud altitude and N increase. Their fluxes vary considerably with D_{eq} and IWC. For N = 1, the flux for the 12-km cloud (open square solid line) is 82 $W*m^{-2}$ (D_{eq} = 93 µm IWC = 0.014 $g*m^{-3}$) with an upper limit of 93 $W*m^{-2}$ (D_{eq} = 75 µm IWC = 0.005 $g*m^{-3}$) and a lower limit of 72 $W*m^{-2}$ (D_{eq} = 110 µm IWC = 0.029 $g*m^{-3}$).

In Figure 4b, the fluxes show similar behavior. The water cloud fluxes decrease with cloud base altitude. The variation with R_{eq} is less than 2 $W*m^{-2}$. The ice cloud fluxes are bunched as before. The small cloud fluxes do not vary greatly from the clear sky case and the large cloud fluxes have more variation.

The errors for the flat plate and black cloud approximations are defined as

$$\delta F^{\uparrow\downarrow} = F^{\uparrow\downarrow} \text{ (approximation)} - F^{\uparrow\downarrow} \qquad (3)$$

The flat plate approximation was used for ice clouds; the black cloud approximation was used for water clouds. The error in the approximations for downward flux at the surface is shown in Figures 5a and b. There is no error for the clear sky case; the lines were not extended to zero at N = 0 in order to increase clarity.

In Figure 5a (TRP) the errors are quite small, less than 1 $W*m^{-2}$. For ice clouds, this is expected since they have little effect on the surface flux. For water clouds, the black cloud approximation works because the downward emission by the water clouds is augmented by the downward reflection of upward flux at the cloud bottom. This can be

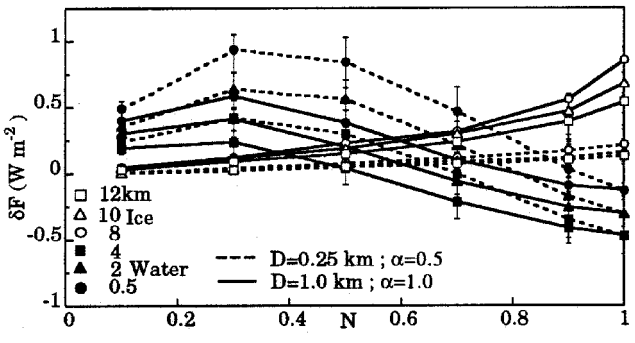

Figure 5a. Tropical downward flux error at surface for various cloud geometries and altitudes.

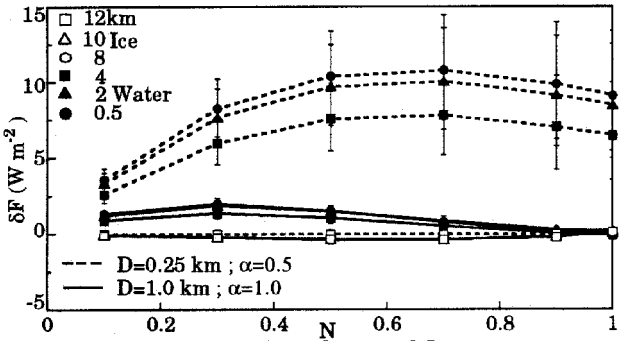

Figure 5b. Sub-arctic winter downward flux error at surface for various cloud geometries and altitudes.

seen by noting that the error is slightly negative at N = 1; the water cloud emissivity is larger than 1. The high temperature and water vapor concentration in the first kilometer mask the scattering effect at the surface.

In Figure 5b (SAW), the errors are less than 2 $W*m^{-2}$, except for the small water clouds. The maximum error for these clouds approaches 15 $W*m^{-2}$. The error decreases as cloud height increases and R_{eq} decreases, peaking at N = 0.5 or 0.7. For N = 0.7, the 0.5-km cloud (solid circle dashed) R_{eq} = 5 µm (the error is 10 $W*m^{-2}$ with an upper limit of 15 $W*m^{-2}$ for R_{eq} = 10 µm and lower limit of 7 $W*m^{-2}$ for R_{eq} = 3 µm). These clouds are no longer opaque, as can be seen from Figure 3b. Because the cloud is no longer opaque, the reflection from the cloud bottom does not augment the downward emission as in Figure 5a. As a result, the black cloud approximation fails.

The errors for the upward flux at 15 km are shown in Figures 6a and b. In Figure 6a (TRP), the water cloud error increases with N and cloud height, with larger clouds having more error. The black cloud approximation overestimates the flux above the clouds. Unlike the surface fluxes, there is no reflection from the cloud top to compensate for the lower emission by the cloud. There is very little error in the flat plate approximation for the small ice clouds (< 0.5 $W*m^{-2}$). This is expected since the clouds are relatively flat, $\alpha = 0.5$. Since the clouds are small, their lower optical thickness improves the accuracy of the flat plate approximation. As α and cloud size increase, the flat plate approximation becomes less accurate. For the large ice clouds, errors increase to a peak at N = 0.5 or 0.7, then decrease. The errors are largest for D_{eq} = 110 µm IWC = 0.029 $g*m^{-3}$ and smallest for D_{eq} = 75 µm IWC = 0.005 $g*m^{-3}$.

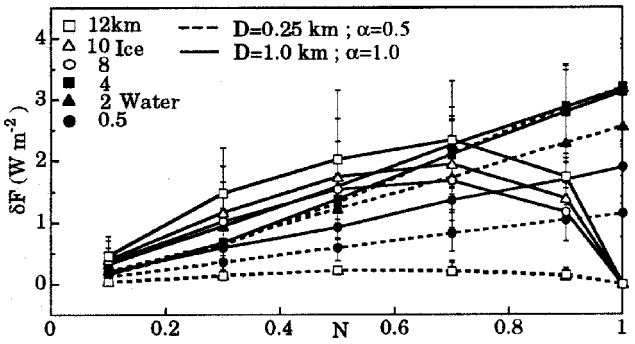

Figure 6a. Tropical upward flux error at 15 km for various cloud geometries and altitudes.

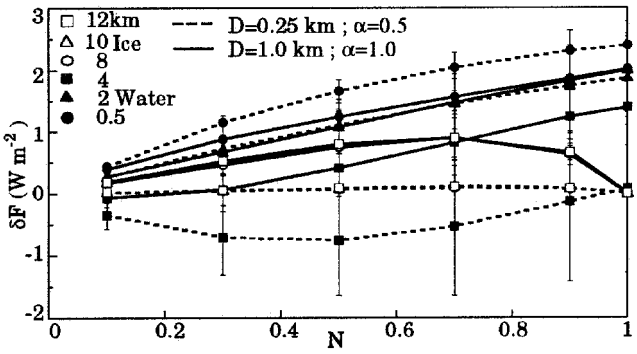

Figure 6b. Sub-arctic winter upward flux error at 15 km for various cloud geometries and altitudes.

Figure 6b (SAW) shows a similar pattern. The flat plate approximation works well for the ice clouds. The error for small clouds is under 0.5 $W * m^{-2}$. The large cloud errors are under 1.5. The black cloud approximation overestimates the flux, but since the temperatures are relatively low, the error is smaller than in Figure 6a. The optical thickness of the small water cloud at 4 km (solid square, dashed line) is small enough to allow transmission from below the cloud. As a result, the black cloud approximation underestimates the flux.

The downward flux errors below the cloud layer and the upward flux errors above the cloud layer for N = 0.5 are shown in Figures 7a and b (TRP) and 8a and b (SAW). The small and large clouds are separated, and the 2 km and 12 km clouds are eliminated to increase clarity. The symbols and curves are for R_{eq} = 5 μm and D_{eq} = 93 μm IWC = $0.014 g * m^{-3}$.

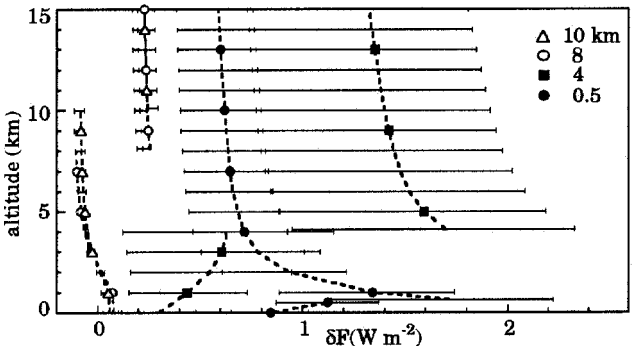

Figure 7a. Tropical flux error profiles for D = 0.25 km; α = 0.5; N = 0.5, various cloud altitudes.

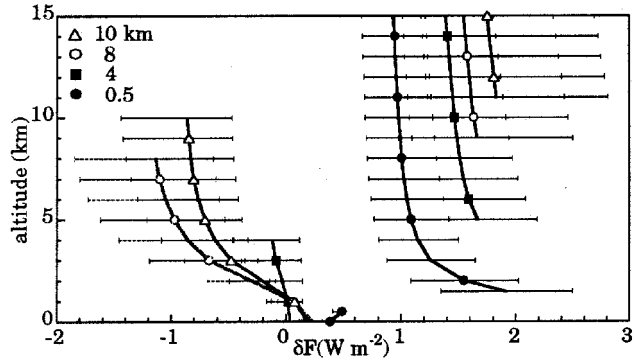

Figure 7b. Tropical flux error profiles for D = 1 km; α = 1; N = 0.5, various cloud altitudes.

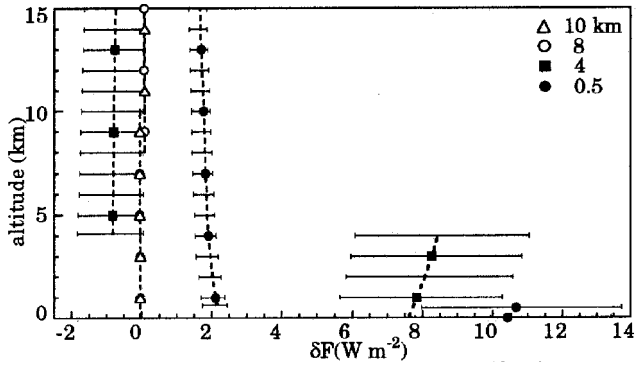

Figure 8a. Sub-arctic winter flux error profiles for D = 0.25 km; α = 0.5; N = 0.5, various cloud altitudes.

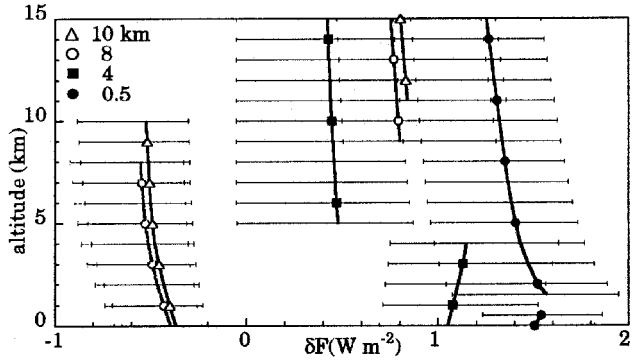

Figure 8b. Sub-arctic winter flux error profiles for D = 1 km; α = 1; N = 0.5, various cloud altitudes.

Except for the water cloud downward flux errors in Figure 8a, the approximations work quite well; the errors are less than 2 $W*m^{-2}$. The errors are largest immediately above or below the cloud. They decrease as distance from the cloud layer increases because the absorbing atmosphere masks the effect of scattering by the cloud layer. This is especially noticeable in the first two kilometers of Figures 7a and b.

Summary and Conclusions

The flat plate approximation worked well for the ice clouds considered; it was most accurate for the small flat clouds. The black cloud approximation worked well for water clouds except in one case where the cloud optical thickness was too small to give a compensating reflection. Cloud scattering effects are largest immediately above and below the cloud layer. Gaseous absorption and emission mask scattering effects. Errors due to neglecting cloud scattering decrease as the distance from the cloud layer increases; the reduction occurs most rapidly below 3 km.

While the approximations work reasonably well for this set of clouds, additional cases should be examined. In particular, models for cloud types with different optical properties, other cloud layer geometric parameterizations, and additional atmospheric conditions should be examined.

Acknowledgments

This paper was sponsored in part by the U.S. Department of Energy's Atmospheric Radiation Measurement (ARM) Program under grant DEFG0294ER61746.

References

Ellingson, R. G. 1982: On the effects of cumulus dimensions on longwave irradiance and heating rates. *J. Atmos. Sci*., **39**, 886-896.

Fu, Q., and K. N. Liou, 1993: Parameterization of the radiative properties of cirrus clouds. *J. Atmos. Sci*., **50**, 2008-2025.

Harshvardhan, and J. A. Weinman 1982: Infrared radiative transfer through a regular array of cuboidal clouds. *J. Atmos. Sci*., **39**, 431-439.

Hu, Y. X., and K. Stamnes, 1993: An accurate parameterization of the radiative properties of water clouds suitable for use in climate models. *J. Clim.*, **6**, 728-742.

Killen, R. M., and R. G. Ellingson 1994: The effect of shape and spatial distribution of cumulus clouds on longwave irradiance. *J. Atmos. Sci*., **51**, 2123-2136.

Takara, E. E., and R. G. Ellingson, 1996: Scattering effects on longwave fluxes in broken cloud fields. *J. Atmos. Sci*., **53**, 1464-1476.